Bulgarian Chemical Communications, Volume 58, Issue 4 (pp. 451-460) 2026 *DOI: 10.34049/bcc.58.4.5743*

Unveiling breast cancer therapeutics of bufadienolides from *Helleborus foetidus* through molecular docking, molecular dynamics, and MMGBSA computations

H. D. Nguyen*

Faculty of Biology, Thai Nguyen University of Education, 24124, Thai Nguyen, Vietnam

Received: January 18, 2026; Revised: May 29, 2026

Breast cancer emerges as the predominant malignancy among women worldwide and ranks as the primary contributor to cancer fatalities in this group. Natural substances derived from plants, particularly bufadienolides, show substantial potential in cancer therapy by inducing apoptosis in malignant cells through multiple signaling pathways. These agents frequently interfere with anti-apoptotic mechanisms, presenting opportunities for addressing breast tumors. The present investigation examined the anti-breast cancer capabilities of bufadienolides isolated from *Helleborus foetidus*, with a focus on their binding to Bcl-2 (PDB: 6GL8). Findings reveal that hellefoetin F (CPD2) facilitates apoptosis through Bcl-2 suppression, achieving a docking binding energy of approximately -7.67 kcal/mol, which surpasses paclitaxel's -6.54 kcal/mol. In 100 ns molecular dynamics simulations, the CPD2-6GL8 complex maintained stability, with RMSD ranging 0.15-0.23 nm (average 0.19 nm), Rg of 1.42-1.48 nm, 0-4 hydrogen bonds, and SASA of 80-95 nm^2. MMGBSA assessments indicated a binding affinity of -27.56 ± 4.68 kcal/mol for CPD2, compared to paclitaxel's -30.47 ± 7.3 kcal/mol. These findings position CPD2 as a prospective Bcl-2 inhibitor for breast cancer therapeutics.

Keywords: Apoptosis; Bcl-2; Breast cancer; Bufadienolides; Molecular docking

INTRODUCTION

Breast cancer is indeed the most frequently diagnosed cancer and the leading cause of cancer death in women globally. It accounts for about one in four new cancer cases in women worldwide, and it is the leading cause of cancer mortality, with an estimated 670,000 deaths in 2022 [1]. Significant research efforts are continuously advancing the understanding of breast cancer across several key areas, including prevention, early detection, diagnosis, and treatment [2, 3]. Ongoing research in targeted cancer therapies focuses on overcoming drug resistance and enhancing treatment efficacy by developing innovative strategies, such as targeted drug delivery systems and combination therapies. Other areas of research include developing new monoclonal antibodies and small-molecule drugs, creating cancer vaccines, and leveraging advancements in areas like gene therapy and nanomedicine to make treatments more precise and practical, with fewer side effects than traditional chemotherapy [4, 5]. Apoptosis, or programmed cell death, is essential for development and tissue homeostasis, and is characterized by specific morphological and biochemical changes, including membrane blebbing, cell shrinkage, and DNA fragmentation. Anti-apoptosis in breast cancer refers to the ability of cancer cells to evade programmed cell death, or apoptosis, which allows them to survive and proliferate uncontrollably. This resistance is a key factor in tumor development, treatment resistance, and recurrence. Breast cancer cells achieve this by manipulating signaling pathways, overexpressing anti-apoptotic proteins like Bcl-2 and Mcl-1, and increasing the expression of genes that promote cell survival [6, 7]. Recent research extensively explores natural bioactive compounds from medicinal plants as promising alternatives or complements to traditional chemotherapy for cancer treatment. These compounds target key cellular mechanisms, primarily by modulating the interconnected pathways of autophagy and apoptosis, offering a promising avenue for modulating these cellular processes, which are crucial in both cancer development and regulation [8, 9].

Bufadienolides are a group of steroid compounds found in both animal and plant sources, which possess significant cardiac, neurotoxic, and anticancer properties. They are known for their ability to inhibit the Na^+-K^+-ATPase pump, which is key to their cardioactive effects, and they can also trigger apoptosis, autophagy, and cell cycle arrest in cancer cells [10, 11]. A previous study reported the isolation of bufadienolides from the species *Helleborus foetidus,* possessing potential cytotoxic activity against the MCF-7 breast cancer cell line [12]. However, the molecular mechanisms underlying its activity remain unexplored. *In silico* drug design, or computer-aided drug design, is a promising approach because it helps overcome the major disadvantages of traditional methods, including high costs, long timelines, and high failure

* To whom all correspondence should be sent:
E-mail*: hungnd@tnue.edu.vn*

© 2026 Bulgarian Academy of Sciences, Union of Chemists in Bulgaria

rates due to late-stage toxicity and efficacy issues [13]. Therefore, this study aimed to better understand the mechanism of the anti-breast cancer potency of selected bufadienolides from *H. foetidus* as natural anticancer agents by targeting the Bcl-2 protein. Looking ahead, future studies should focus on confirming these results through *in vitro* and *in vivo* experiments, thoroughly mapping out the underlying biochemical mechanisms, and optimizing delivery systems to translate the discoveries into practical therapeutic applications.

MATERIALS AND METHODS

Structural preparation of selected ligands

The list of bufadienolides possessing anti-cancer activity against the MCF-7 breast cancer cell line was collected in the previous study [12]. For details, the selected ligands, including hellebrigenin-3-*O*-β-D-glucopyranoside (CPD1) and hellefoetin F (CPD2), have molecular formulas of $C_{30}H_{42}O_{11}$ and $C_{24}H_{30}O_6$, respectively, with molecular weights of 578.2727 and 414.2042 *m/z*. The Paclitaxel, possessing a molecular formula of $C_{47}H_{51}NO_{14}$ and a molecular weight of 853.3310 *m/z*, was chosen as the comparative reference (Figure 1).

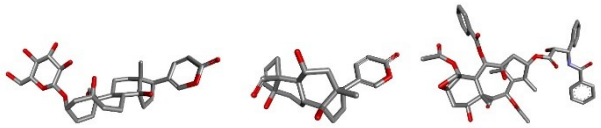


Figure 1. 3D Structures of selected ligands. (A) CPD1, (B) CPD2, and (C) Paclitaxel.

Molecular docking analysis

The three-dimensional configurations of the selected ligands were generated in PDB format using Biovia Discovery Studio Visualizer, which incorporates polar hydrogen atoms, calculates Gasteiger partial charges, and permits flexibility in all torsional bonds. The Bcl-2 target protein structure (PDB code: 6GL8) was retrieved in PDB format from the RCSB Protein Data Bank [14]. During receptor preparation, crystallographic water molecules were removed in BIOVIA Discovery Studio to comply with the AutoDock-based docking protocol, which does not explicitly model interfacial waters. Ligand-protein docking simulations were carried out using AutoDock Tools, with a grid box sized at 60 points along each x, y, and z dimension and a grid point separation of 0.375 Å. The binding pocket coordinates on the 6GL8 structure were set to x = 9.866 Å, y = 0.590 Å, and z = 16.717 Å. To identify the lowest-energy ligand-protein poses that favored strong interactions, the Lamarckian genetic algorithm was applied. Upon finishing the docking process, the pose with the highest binding strength was chosen for analysis in Discovery Studio Client 2024 and then benchmarked against the docking outcomes of Paclitaxel, serving as a reference standard on the identical protein, to assess comparative binding characteristics [15].

Molecular dynamics simulation

Molecular dynamics were conducted on the optimal docked pose interacting with the 6GL8 protein over a 100 ns timeframe, employing GROMACS version 2024.4 software [16]. The CHARMM36 force field was applied to describe molecular mechanics. The protein structure underwent refinement to fill in absent atoms and residues through Swiss-PdbViewer [17]. Ligand topologies were created using SwissParam [18]. For solvation, the protein-ligand assembly was placed within a triclinic box under periodic boundary conditions across all three dimensions, utilizing the SPC water model along with 0.15 M sodium chloride. Thus, solvent molecules were treated explicitly in MD, allowing interfacial water reorganization around the ligand–protein interface during the simulation. Optimization and charge neutralization of the structure were achieved via 50,000 energy minimization steps utilizing the steepest descent algorithm. System equilibration proceeded with a 200 ps NVT phase, followed by a 200 ps NPT phase, at a temperature of 300 K and a pressure of 1.0 bar. Temperature control was maintained by the V-rescale thermostat (coupling constant τt = 0.1 ps) applying separate coupling groups for the protein-ligand complex and the solvent. Pressure regulation during the NPT phase utilized the Berendsen barostat with isotropic coupling (τp = 2.0 ps, compressibility = 4.5×10^{-5} bar^{-1}). For non-bonded interactions, the Verlet cutoff scheme was applied with a neighbor-list cutoff (rlist) of 1.2 nm. Short-range electrostatic interactions were truncated at 1.2 nm, whereas long-range electrostatics were computed using the Particle Mesh Ewald (PME) method. Van der Waals interactions were managed via a force-switch modifier operating between 1.0 nm and 1.2 nm. Each system underwent a single 100 ns production run, transitioning to the Parrinello-Rahman barostat for stable pressure maintenance, with a 2 fs integration step applied, and trajectories saved at 10 ps intervals. Data from these simulations were processed using the Grace software to derive key metrics, including root mean square deviation (RMSD), per-residue root mean square fluctuation (RMSF), radius of gyration (Rg), number of hydrogen bonds (H-

bonds), and solvent-accessible surface area (SASA). To gauge the stability of conformations in the bound complexes, UCSF Chimera version 1.13.3 was used for structural alignments. By overlaying ligand poses from 0 ns and 100 ns against the protein's active site, the consistency of engagements with critical residues, encompassing hydrogen bonds, van der Waals contacts, and hydrophobic effects, could be examined across the entire simulation. This methodology provided a deeper understanding of the evolving dynamics and robustness of the interaction between ligands and the protein over a 100 ns period.

Molecular mechanics generalized Born surface area (MMGBSA) analysis

The MMGBSA calculations were executed through the gmx_MMPBSA tool, applying the charmm36 force field to evaluate the binding free energies of the CPD2-6GL8 and Paclitaxel-6GL8 systems. The generalized Born component handles electrostatic contributions to solvation within an implicit solvent environment, whereas non-polar solvation effects are gauged via calculations of the solvent-accessible surface area. Polar solvation influences on electrostatic terms were approximated through the Generalized Born formalism, configuring the internal solute dielectric constant to 1.0 and the exterior solvent dielectric constant to 80.0. In contrast, hydrophobic contributions were derived from computations involving the solvent-accessible surface area (SASA), which is interpreted as an indicator of surface tension at the solute-solvent boundary with an applied surface tension parameter (γ = 0.0072 kcal/mol/Å^2). These energies were computed from molecular dynamics simulation paths, drawing on 125 evenly spaced frames taken every 80 ps across an 80 ns simulation (spanning 20 ns to 100 ns). By averaging these results, the analysis captured the fluctuating nature of ligand-protein associations, offering a clearer view of their binding potency and conformational resilience in a modeled setting. For reproducibility, the MMGBSA analysis in gmx_MMPBSA was conducted using mmpbsa.in together with em.tpr, index.ndx, topol.top, and md_0_10_center.xtc. The corresponding settings were startframe = 2000, endframe = 10000, interval = 80, verbose = 2, and igb = 5.

RESULTS AND DISCUSSION

Molecular docking analysis

Molecular docking is a computational method that utilizes search algorithms to identify the optimal binding pose of a compound within a protein's binding site, and then employs a scoring function to rank these poses based on their predicted binding affinity or energy. This process helps in drug design and discovery by predicting how well a potential drug will bind to its target [19]. This study assessed the binding affinities and molecular interactions of selected compounds with the Bcl-2 protein (PDB: 6GL8), using Paclitaxel as a comparative reference. Before production docking, the protocol was validated by redocking the co-crystallized ligand and comparing the regenerated pose with the crystallographic conformation. This procedure yielded an RMSD of 0.7540 Å (Figure 2), indicating close pose reproduction. RMSD values below 2 Å are commonly used as a practical criterion for acceptable docking performance [20]. Following validation, candidate binding poses were ranked by docking score and the lowest-scoring conformations were selected for downstream interaction assessment.

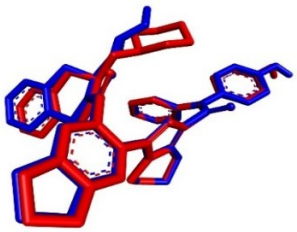


Figure 2. Superimposition of the docked and native ligands for validation of the molecular docking protocol on protein 6GL8 (red = native, blue = docked)

Details of how these compounds engage with the binding sites on 6GL8 are shown in Table 1 highlighting the amino acids involved and their positions within the ligand interaction zone. Docking simulations identified key non-covalent forces, including hydrogen bonding, van der Waals forces, and hydrophobic interactions between the protein and the selected ligands.

The compounds CPD1 and CPD2 showed distinct engagement profiles with the Bcl-2 protein, which plays a critical role in regulating cell death pathways relevant to cancer progression. For CPD1, a total of 13 interactions were observed, including 2 hydrogen bonds (Arg129, Arg146), 4 van der Waals connections (Tyr108, Gln118, Glu136, Leu137), and 7 hydrophobic links (Phe104, Phe112, Met115, Leu119, Val133, Ala149, Phe153) (Figure 3A). The active site residues contributing to these included Phe104, Tyr108, Phe112, Gln118, Leu137, Arg146, Ala149, and Phe153. The binding strength for the CPD1-6GL8 pair was recorded at -6.26 kcal/mol.

In contrast, CPD2 formed 10 interactions in all, featuring 2 hydrogen bonds (Gln118, Glu136), 4 van der Waals interactions (Phe104, Arg129, Ala149, Phe153), and 4 hydrophobic associations (Met115, Leu119, Val133, Leu137) (Figure 3B). Residues at the active sites encompassed Phe104, Gln118,

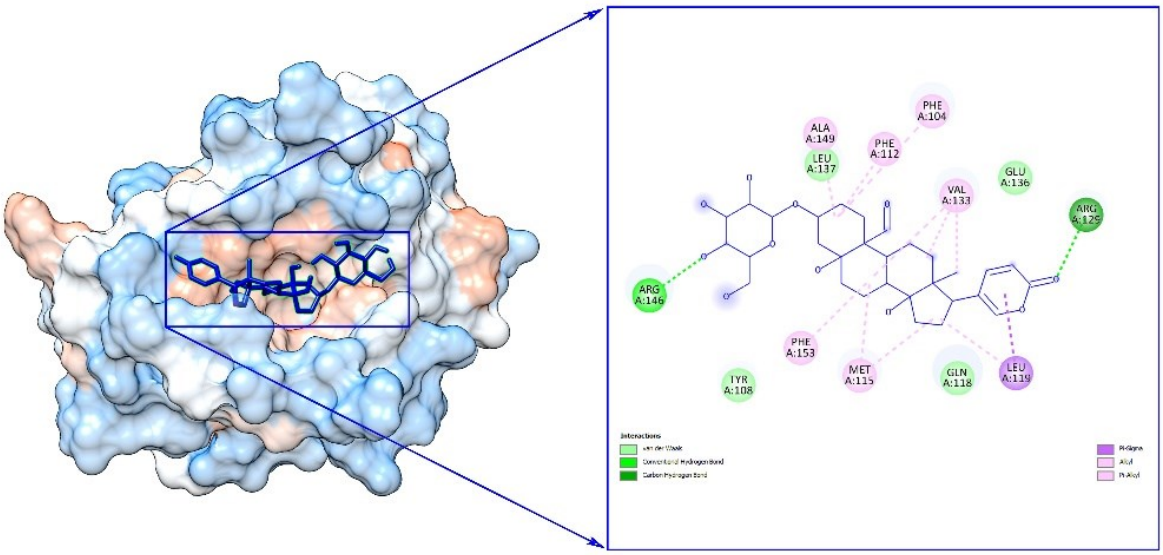
Leu137, Ala149, and Phe153. This resulted in a binding energy of approximately -7.67 kcal/mol for the CPD2-6GL8 complex, suggesting a relatively stable arrangement.

Paclitaxel, serving as the control ligand, produced 15 interactions overall, with 2 hydrogen bonds (Gln118, Glu136), 11 van der Waals contacts (Phe104, Tyr108, Asp111, Phe112, Thr132, Val133, Leu137, Arg146, Ala149, Glu152, Phe153), and 2 hydrophobic interactions (Leu119, Met115). The active sites involved Phe104, Tyr108, Asp111, Phe112, Gln118, Leu137, Arg146, Ala149, and Phe153 (Figure 3C). Its binding energy with 6GL8 was approximately -6.54 kcal/mol. Although Paclitaxel demonstrated solid interaction potential, its binding value was less favorable and involved fewer hydrophobic elements compared to CPD2, implying a somewhat lower overall affinity than the top-performing compound.

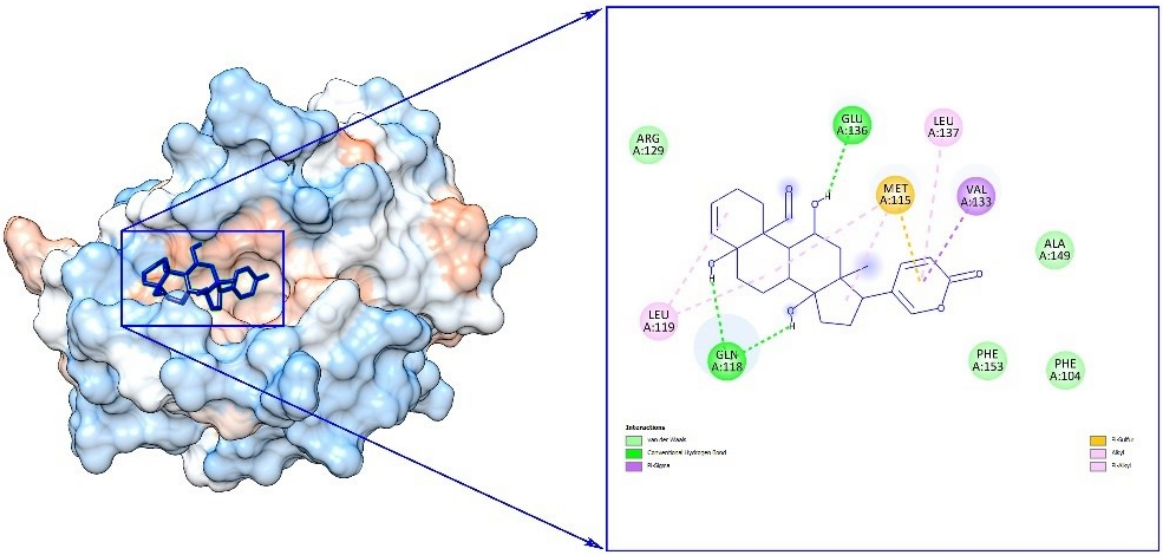
To further validate the computational protocol against empirical measurements, the docking score of the control ligand, Paclitaxel, was compared with its established experimental binding affinity toward Bcl-2. Previous biosensor kinetic analyses have demonstrated that Paclitaxel directly binds to the Bcl-2 protein with an experimental dissociation constant of 5.4 μM (approximately of -7.18 kcal/mol) [21]. The computationally derived docking score for Paclitaxel in the present study (-6.54 kcal/mol) exhibits close agreement with this experimental benchmark. This alignment between in silico predictions and *in vitro* functional data robustly confirms the reliability and accuracy of the utilized docking parameters and scoring function for assessing ligand affinities within the targeted binding pocket.

Table 1. The interactions between the docked ligands and the protein 6GL8.

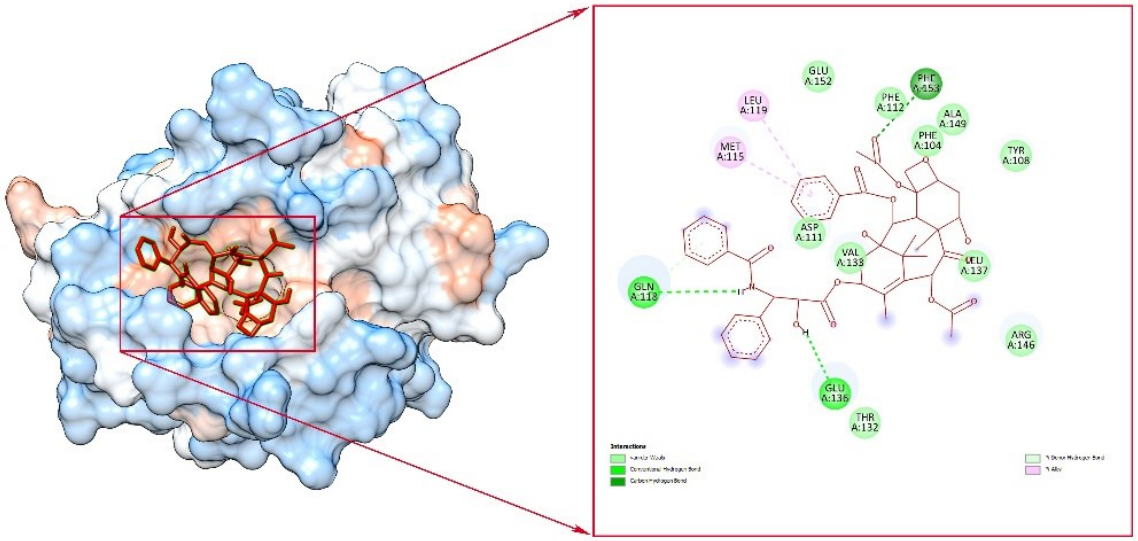
Docked ligands	Binding energy (kcal/mol)	Hydrogen bond interaction	Van der Waals interaction	Hydrophobic interaction
CPD1	-6.26	Arg129, Arg146	Tyr108, Gln118, Glu136, Leu137	Phe104, Phe112, Met115, Leu119, Val133, Ala149, Phe153
CPD2	-7.67	Gln118, Glu136	Phe104, Arg129, Ala149, Phe153	Met115, Leu119, Val133, Leu137
Paxlitaxel	-6.54	Gln118, Glu136	Phe104, Tyr108, Asp111, Phe112, Thr132, Val133, Leu137, Arg146, Ala149, Glu152, Phe153	Leu119, Met115



A



B



C

Figure 3. Molecular docking model and 2D interaction diagram of CPD1 (A), CPD2 (B), and Paclitaxel (C) with 6GL8 protein

Docking evaluations of these compounds against Bcl-2 revealed diverse non-covalent binding mechanisms, such as hydrogen bonds, van der Waals forces, and hydrophobic interactions, all of which enhance the structural integrity of the resulting complexes [22]. Hydrogen bonds provide targeted, strong connections through electron-sharing between atoms, such as oxygen or nitrogen. Hydrophobic interactions arise from the tendency of nonpolar regions to aggregate in water-based environments, thereby reducing exposure to solvents and promoting tighter associations. While hydrogen bonds offer precision and potency, hydrophobic forces deliver broad-based support, particularly over larger contact areas. Van der Waals attractions further strengthen these setups by facilitating close-range alignments that work in tandem with other forces to boost overall binding efficiency. More negative binding energies typically signal greater complex resilience and better ligand retention at the target site [23].

CPD2 was chosen for further molecular dynamics exploration due to its standout docking results with the 6GL8 protein, characterized by the strongest binding energy of -7.67 kcal/mol and meaningful active site involvement through 10 interactions, including 2 hydrogen bonds, 4 van der Waals contacts, and 4 hydrophobic interactions. This performance outperforms CPD1 (-6.26 kcal/mol) and Paclitaxel (-6.54 kcal/mol), making CPD2 the leading option for probing long-term stability and interaction durability in the Bcl-2 pocket. Prioritizing CPD2 enables an in-depth examination of structural changes, energetic profiles, and key

residue roles across simulation durations, while maintaining Paclitaxel as a standard for assessing potential in modulating apoptosis for cancer treatment strategies.

Molecular dynamics simulation

Molecular dynamics simulation is a powerful computational method that simulates the physical movements of atoms and molecules over time to investigate conformational changes in systems, such as protein-ligand complexes. By solving classical equations of motion, MD provides a virtual microscope to study how molecules fluctuate, their dynamics, and how a ligand interacts with a receptor, offering atomic-level insights into biological processes. This technique is used in fields like computational biology for drug discovery, protein folding, and understanding protein-ligand docking [24]. Therefore, the evaluation systematically investigated RMSD, RMSF, Rg, hydrogen bond formation, and SASA metrics to determine the stability, flexibility, and solvent exposure of the CPD2-6GL8 and Paclitaxel-6GL8 complexes throughout the simulation timeframe.

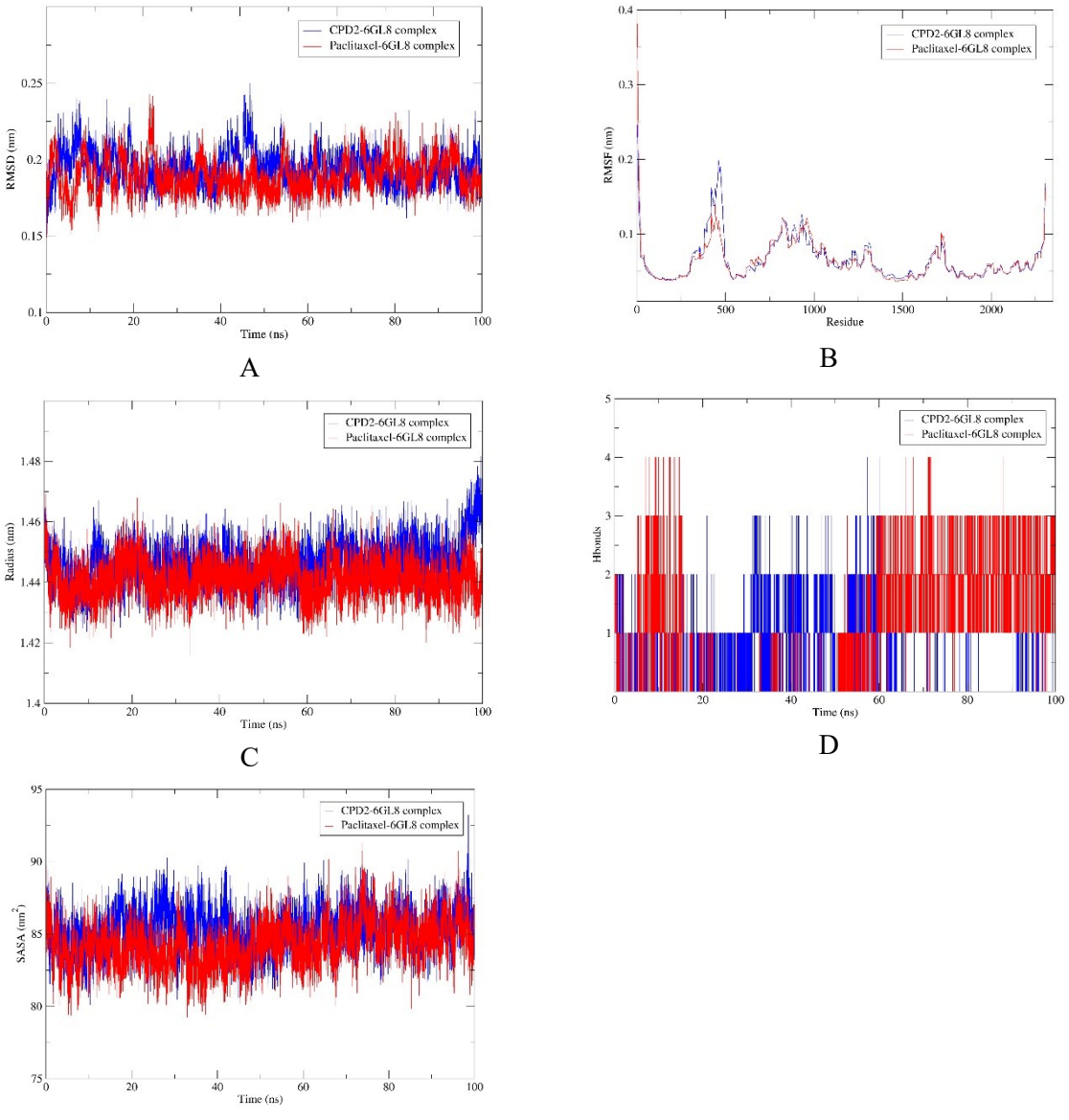


Figure 4. Results of MD simulation for the bindings of CPD2 (blue) and Paclitaxel (red) with 6GL8 protein. (A) RMSD, (B) RMSF, (C) Rg, (D) Hbonds, (E) SASA

The RMSD in molecular dynamics is a measure of the average distance between the atoms of superimposed molecules, quantifying the extent to which a structure has changed from a reference structure over time. It is calculated by comparing the coordinates of atoms in different frames of a simulation to a reference structure, most commonly the initial frame. A low RMSD indicates that the molecule has remained in a similar conformation, while a high RMSD suggests significant structural changes [25]. Across the 100 ns timeframe, the RMSD profiles for the CPD2-6GL8 and Paclitaxel-6GL8 pairings displayed highly comparable stabilization trends (Figure 4A). The CPD2-6GL8 combination exhibited RMSD readings primarily ranging from 0.15 to 0.23 nm, yielding an average of approximately 0.19 nm, which suggests impressive structural rigidity and solid attachment within the 6GL8 pocket. On the other hand, the Paclitaxel-6GL8 interaction showed RMSD spans of 0.15 to 0.25 nm, averaging approximately 0.20 nm. Because these averages strongly coincide within their respective standard deviations, the slight numerical difference is not statistically significant. Rather than indicating enhanced spatial reliability for one complex over the other, these overlapping evolutions demonstrate that both systems achieve equivalent structural equilibrium. Taken together, the RMSD observations confirm that the CPD2-6GL8 complex maintains its baseline framework with a level of stability entirely on par with the established reference, Paclitaxel, throughout the simulation.

The RMSF is a measure used in molecular dynamics to quantify the flexibility of a biomolecule by calculating the average deviation of each atom's position from its average position over time. It provides information about how much individual atoms or residues fluctuate during a simulation; high RMSF values indicate high flexibility, while low values indicate stability and rigidity. This analysis is often used to identify flexible regions of proteins, which can be important for understanding protein function and allosteric mechanisms. As shown in Figure 4B, the RMSF for the CPD2-6GL8 and Paclitaxel-6GL8 systems, focusing on residues Gly7 through Gly203, displays readings generally between 0.05 and 0.2 nm. In the CPD2-6GL8 complex, RMSF holds steady at roughly 0.1 nm over much of this segment, pointing to restrained fluctuations and enhanced structural steadiness, likely influenced by interactions near binding hotspots like Phe104, Leu137, and Phe153. The Paclitaxel-6GL8 profile follows suit, averaging about 0.1 nm with occasional alignments and subtle drops, implying equivalent levels of constraint. This consistent profile across both pairings underscores the ligands' role in fortifying the protein, which in turn bolsters engagements in its operational domains.

The Rg value in molecular dynamics is a measure of how an object's mass is distributed around an axis of rotation. It is the distance from the axis at which the entire mass could be concentrated without changing the object's moment of inertia. In the context of molecular dynamics simulations, a higher Rg indicates a more expanded and less compact structure, while a lower Rg suggests a more compact and stable structure [26]. As shown in Figure 4C, Rg trajectories for the CPD2-6GL8 and Paclitaxel-6GL8 complexes are tracked over a 100 ns period. Each displays consistent undulations between 1.42 and 1.48 nm, averaging roughly 1.45 nm, indicating that the 6GL8 protein maintains a well-organized conformation when complexed in these scenarios throughout the entire run.

In molecular dynamics, the Hbonds are determined by analyzing simulation trajectories using specific criteria. This involves identifying hydrogen atoms, donor heavy atoms, and acceptor atoms within a certain distance and angular range. The total number is then calculated by counting the instances that meet these criteria, and can also be analyzed for specific interactions between molecules or within a single molecule [27]. Across a 100 ns simulation, the CPD2-6GL8 complex shifted between 0 and 4 bonds, paralleling the Paclitaxel-6GL8 range of 0 to 4 bonds (Figure 4D). This ongoing presence reflects firm lodging in the 6GL8 protein's active region throughout, where the CPD2-6GL8 complex generally sustained around 3 bonds on average, edging out Paclitaxel-6GL8's approximate 2 bonds. Crucially, a comparative evaluation between the dynamic trajectories and the static docking poses revealed high consistency in the interaction profiles. Trajectory analysis confirmed that the primary hydrogen bonds initially identified in the docking phase, specifically engaging residues Gln118 and Glu136 for both the CPD2 and Paclitaxel complexes, were heavily preserved throughout the 100 ns timeframe. The observed fluctuations in the total number of hydrogen bonds (spanning 0 to 4) represent the dynamic breaking and reforming of these essential core interactions, combined with the occasional formation of transient bonds with neighboring amino acids. The variation emphasizes CPD2's edge in forging more robust associations with the 6GL8 protein.

The SASA measures the surface of a molecule accessible to solvent molecules, providing insights into conformational changes, protein folding, and

interactions. It's calculated by simulating a "probe" sphere, representing a solvent molecule, rolling over the molecule's van der Waals surface. Analyzing changes in SASA over time is crucial for understanding a molecule's behavior during a simulation, such as how a protein folds or how a ligand binds to its receptor. In this case, SASA profiles were monitored for the CPD2-6GL8 and Paclitaxel-6GL8 pairings to explore changes in their solvent interaction patterns. During the 100 ns period, each showed persistent variations, ranging from approximately 80 to 95 nm², with an average of nearly 87 nm² (Figure 4E). These fluctuations indicate minor adjustments in protein-solvent contacts induced by the ligands, which may impact the durability of their binding. The similar spans and mean values across both setups highlight an even solvent engagement, indicating strong resilience within the 6GL8 pocket, even with varying ligand characteristics.

In summary, this comprehensive assessment of dynamic parameters, including RMSD, RMSF, Rg, and SASA, demonstrates that the CPD2-6GL8 complex achieves a conformational equilibrium and overall structural stability that is highly comparable to the established Paclitaxel-6GL8 reference system. Both complexes maintain a compact, well-organized framework with consistent solvent exposure profiles throughout the 100 ns simulation timeframe. While CPD2 exhibits a slight edge in the average number of sustained hydrogen bonds, the collective dynamic metrics indicate equivalent levels of spatial restraint and system resilience. These substantiated observations confirm that CPD2 does not necessarily exceed, but rather successfully matches the control ligand's capability to form firm, durable, and stable interactions within the active pocket of the 6GL8 protein.

Free binding energy (MMGBSA) analysis

Molecular mechanics generalized Born surface area (MMGBSA) is a computational method used in herbal medicine research to predict the binding affinity of a plant's bioactive compounds to a specific protein target. By calculating the free energy of binding, researchers can identify and validate which compounds from herbal extracts have the potential to be effective drug candidates for a particular disease, supporting traditional use with molecular-level evidence. This method is part of a larger workflow that includes molecular docking and molecular dynamics simulations [28]. The MMGBSA method was used to approximate the binding free energies in these ligand-protein pairings, relying on the gmx_MMPBSA software in conjunction with the CHARMM36 force field. Snapshots from the entire molecular dynamics trajectories, covering an 80 ns interval, underwent this evaluation. For each complex, the binding free energy (ΔG_bind) is expressed as ΔG_bind = G_complex - (G_receptor + G_ligand), where G_receptor denotes the energy of the isolated receptor and G_ligand that of the free ligand. Alternatively, it breaks down into ΔG_bind = ΔH - TΔS, where ΔH represents the enthalpy change and -TΔS captures the entropic penalty associated with the binding. By excluding entropy, the result provides a relative energy estimate suitable for gauging affinities across similar systems. This examination covered the 80 ns segment, using 125 frames extracted at 80 ps intervals (20 to 100 ns). The process delivered averaged energies that incorporate the fluid aspects of the associations, giving indications of ligand potency and resilience in an emulated physiological context. Results from the MMGBSA calculations for the pairings appear in Table 2.

Table 2. Free energy of binding obtained using MMGBSA calculations.

Energy component	Average (kcal/mol)		Standard deviation	
	CPD2-6GL8	Paclitaxel-6GL8	CPD2-6GL8	Paclitaxel-6GL8
ΔVDWA	-34.24	-42.48	4.51	6.30
ΔALS				
ΔEEL	-13.03	-14.58	10.07	10.50
ΔEGB	24.11	32.31	7.64	8.78
ΔESURF	-4.40	-5.71	0.57	0.93
ΔGGAS	-47.27	-57.06	10.11	14.27
ΔGSOLV	19.71	26.59	7.56	8.16
ΔTOTAL	-27.56	-30.47	4.68	7.30

These MMGBSA-based binding free energies align with the structural stabilization observed in the molecular dynamics trajectories, revealing that the binding affinities of both complexes are highly comparable. Although the mean total binding free energy (ΔGbind) for Paclitaxel-6GL8 (-30.47 ± 7.30 kcal/mol) is numerically lower than that of CPD2-6GL8 (-27.56 ± 4.68 kcal/mol), these average values clearly coincide within their respective standard deviations. Consequently, the slight numerical difference is not statistically significant, indicating that both ligands possess equivalent binding strengths. A closer inspection of the energy components shows that while Paclitaxel exhibits somewhat higher mean enthalpic contributions, such as van der Waals (-42.48 kcal/mol) and electrostatic (-14.58 kcal/mol) interactions, compared to CPD2 (-34.24 and -13.03 kcal/mol, respectively), the overall thermodynamic profiles of both systems represent highly stable associations. Consistent with the dynamic metrics (RMSD, RMSF, Rg, and SASA),

these thermodynamic indicators conclusively demonstrate that CPD2 establishes a firm, steady, and thermodynamically favorable linkage within the 6GL8 active site that is entirely on par with the established control drug, Paclitaxel.

CONCLUSION

This study provides a detailed computational exploration of bufadienolides sourced from *H. foetidus* as potential suppressors of breast cancer through interaction with the Bcl-2 protein (6GL8), which is essential in regulating programmed cell death. CPD2 stood out with a solid docking energy (-7.67 kcal/mol) that outpaced Paclitaxel (-6.54 kcal/mol), forming varied connections like hydrogen bonds and van der Waals forces. Dynamics simulations over 100 ns verified the CPD2-6GL8 assembly's steadiness, evidenced by a mean RMSD around 0.19 nm, radius of gyration (Rg) close to 1.45 nm, and roughly 3 hydrogen bonds, modestly outperforming Paclitaxel's 0.21 nm RMSD and about 2 bonds. MMGBSA results demonstrated a secure binding for CPD2 (-27.56 ± 4.68 kcal/mol) compared to Paclitaxel (-30.47 ± 7.3 kcal/mol), aided by van der Waals interactions (-34.24 kcal/mol) and electrostatic interactions (-13.03 kcal/mol). The major advantage of CPD2 lies in its nature as a novel, plant-derived chemical scaffold. Demonstrating in silico binding affinities and complex stabilities that match a highly potent, established chemotherapeutic agent like Paclitaxel highlights CPD2 as a highly valuable lead compound. Because conventional taxane-based therapies often face severe clinical limitations, including neurotoxicity and multi-drug resistance, the discovery of this stable, naturally sourced bufadienolide provides a promising alternative blueprint for drug design. Overall, these outcomes highlight CPD2 as a promising candidate under the modeled computational conditions for breast cancer interventions, encouraging further refinements and potential applications in oncology.

Despite the strong *in silico* evidence supporting CPD2 as a potential Bcl-2 (6GL8) inhibitor, experimental verification is still essential to confirm the accuracy of these predictions. Due to limited laboratory equipment and resources, this study did not include *in vitro* or *in vivo* validation, which represents an important limitation. Future work should prioritize cell-based assays and animal models to evaluate CPD2's biological efficacy, safety, and pharmacological behavior, while also checking for possible off-target or unintended covalent effects. If CPD2 continues to perform well in preclinical testing, it may justify further development toward translational and clinical applications.

REFERENCES

1. F. Bray, M. Laversanne, H. Sung, J. Ferlay, R. L. Siegel, I. Soerjomataram, A. Jemal, *CA. Cancer J. Clin.*, **74**, 229 (2024).
2. E. I. Obeagu, G. U. Obeagu, *Medicine*, **103**, (2024).
3. L. Wilkinson, T. Gathani, *Br. J. Radiol.*, **95**, 20211033 (2022).
4. S. Imtiaz, U. T. Ferdous, A. Nizela, A. Hasan, A. Shakoor, A. W. Zia, S. Uddin, *Eur. J. Med. Chem.*, **290**, 117535 (2025).
5. F. Davodabadi, S. F. Sajjadi, M. Sarhadi, S. Mirghasemi, M. Nadali Hezaveh, S. Khosravi, M. Kamali Andani, M. Cordani, M. Basiri, S. Ghavami, *Eur. J. Pharmacol.*, **958**, 176013 (2023).
6. M. M. Williams, L. Lee, T. Werfel, M. M. M. Joly, D. J. Hicks, B. Rahman, D. Elion, C. McKernan, V. Sanchez, M. V Estrada, S. Massarweh, R. Elledge, C. Duvall, R. S. Cook, *Cell Death Dis.*, **9**, 21 (2018).
7. M. M. Williams, R. S. Cook, *Oncotarget*, **6**, 3519 (2015).
8. [C. Braicu, O. Zanoaga, A.-A. Zimta, A. B. Tigu, K. L. Kilpatrick, A. Bishayee, S. M. Nabavi, I. Berindan-Neagoe, *Semin. Cancer Biol.*, **80**, 218 (2022).
9. [M. A. Rahman, M. A. Hannan, R. Dash, M. D. H. Rahman, R. Islam, M. J. Uddin, A. A. M. Sohag, M. H. Rahman, H. Rhim, *Front. Pharmacol.*, **12,** 639628 (2021).
10. L. J. Deng, Y. Li, M. Qi, J. S. Liu, S. Wang, L. J. Hu, Y. H. Lei, R. W. Jiang, W. M. Chen, Q. Qi, H. Y. Tian, W. L. Han, B. J. Wu, J. X. Chen, W. C. Ye, D. M. Zhang, *Eur. J. Pharmacol.*, **887**, 173379 (2020).
11. Y. Xu, X. Liu, S. Schwarz, L. Hu, D. Guo, Q. Gu, W. Schwarz, *Biochem. Biophys. Reports*, **6**, 158 (2016).
12. J. F. Zong, X. X. Guo, K. K. Zou, C. J. Cui, Z. H. Hu, R. Y. Hou, *Phytochemistry*, **235**, 114476 (2025).
13. [A. Islam, D. Jena, N. S. Mondal, A. Teli, S. Mondal, M. K. Gautam, *Curr. Drug Discov. Technol.*, **22**, (2025).
14. P. Casara, J. Davidson, A. Claperon, G. Le Toumelin-Braizat, M. Vogler, A. Bruno, M. Chanrion, G. Lysiak-Auvity, T. Le Diguarher, J. B. Starck, I. Chen, *Oncotarget*, **9**, 20075 (2018).
15. H. D. Nguyen, *Indian J. Chem.*, **64**, 383 (2025).
16. D. Van Der Spoel, E. Lindahl, B. Hess, G. Groenhof, A. E. Mark, H. J. C. Berendsen, *J. Comput. Chem.*, **26**, 1701 (2005).
17. [N. Guex, M. C. Peitsch, *Electrophoresis*, **18**, 2714 (1997).
18. V. Zoete, M. A. Cuendet, A. Grosdidier, O. Michielin, *J. Comput. Chem.*, **32**, 2359 (2011).
19. A. Tiwari, S. Singh, D. B. Singh, Computational approaches in drug designing (Bioinformatics), Academic Press, Boston, 2022.
20. H. Gohlke, M. Hendlich, G. Klebe, *J. Mol. Biol.*, **295**, 337 (2000).
21. [C. Ferlini, L. Cicchillitti, G. Raspaglio, S.

Bartollino, S. Cimitan, C. Bertucci, S. Mozzetti, D. Gallo, M. Persico, C. Fattorusso, G. Campiani, G. Scambia, *Cancer Res.*, **69**, 6906 (2009).
22. E. J. Millan-Casarrubias, Y. V García-Tejeda, C. H. González-De la Rosa, L. Ruiz-Mazón, Y. M. Hernández-Rodríguez, O. E. Cigarroa-Mayorga, *Curr. Issues Mol. Biol.*, **47**, 193 (2025).
23. M. Majewski, X. Barril, *J. Chem. Inf. Model.*, **60**, 1644 (2020).
24. A. K. Padhi, M. Janežič, K. Y. Zhang, Molecular dynamics simulations: Principles, methods, and applications in protein conformational dynamics (Advances in protein molecular and structural biology methods), Academic Press, Boston, 2022.
25. K. Sargsyan, C. Grauffel, C. Lim, *J. Chem. Theory Comput.*, **13**, 1518 (2017).
26. N. Anwar, F. A. Najam, Understanding cross-sections (Structural cross sections), Butterworth-Heinemann, Oxford, 2017.
27. H. Sun, D. Surblys, H. Matsubara, T. Ohara, *Int. J. Heat Mass Transf.*, **208**, 124091 (2023).
28. J. Xue, X. Huang, Y. Zhu, *RSC Adv.*, **9**, 13868 (2019).